Stable and dynamic cortical electrophysiology of induction and emergence with propofol anesthesia

Jonathan D. Breshears[a], Jarod L. Roland[b], Mohit Sharma[c], Charles M. Gaona[c], Zachary V. Freudenburg[d], Rene Tempelhoff[b,e], Michael S. Avidan[e], and Eric C. Leuthardt[b,c,1]

Departments of [b]Neurological Surgery and [e]Anesthesiology, [a]Washington University School of Medicine, St. Louis, MO 63110; and Departments of [c]Biomedical Engineering and [d]Computer Science and Engineering, Washington University, St. Louis, MO 63130

Edited by Marcus E. Raichle, Washington University, St. Louis, MO, and approved October 27, 2010 (received for review August 13, 2010)

The mechanism(s) by which anesthetics reversibly suppress consciousness are incompletely understood. Previous functional imaging studies demonstrated dynamic changes in thalamic and cortical metabolic activity, as well as the maintained presence of metabolically defined functional networks despite the loss of consciousness. However, the invasive electrophysiology associated with these observations has yet to be studied. By recording electrical activity directly from the cortical surface, electrocorticography (ECoG) provides a powerful method to integrate spatial, temporal, and spectral features of cortical electrophysiology not possible with noninvasive approaches. In this study, we report a unique comprehensive recording of invasive human cortical physiology during both induction and emergence from propofol anesthesia. Propofol-induced transitions in and out of consciousness (defined here as responsiveness) were characterized by maintained large-scale functional networks defined by correlated fluctuations of the slow cortical potential (<0.5 Hz) over the somatomotor cortex, present even in the deeply anesthetized state of burst suppression. Similarly, phase-power coupling between θ- and γ-range frequencies persisted throughout the induction and emergence from anesthesia. Superimposed on this preserved functional architecture were alterations in frequency band power, variance, covariance, and phase–power interactions that were distinct to different frequency ranges and occurred in separable phases. These data support that dynamic alterations in cortical and thalamocortical circuit activity occur in the context of a larger stable architecture that is maintained despite anesthetic-induced alterations in consciousness.

cortical networks | human cortex | gamma rhythms

Every year millions of people undergo general anesthesia, yet the mechanism(s) by which widely used clinical anesthetics reversibly ablate consciousness remains incompletely understood (1). Moreover, the manner in which the brain is able to tolerate global pharmacologic suppression, yet still maintain memories and resume complex cortical interactions that define a person's cognition after removal of this suppression, also remains unknown. Thus far, the majority of studies in humans have used noninvasive methods such as functional imaging and electroencephalography (EEG) to arrive at the current understanding. To date, positron emission tomography (PET) and functional magnetic resonance imaging (fMRI) studies show that there is a complex interplay between and within the thalamus and the cortex. These studies demonstrate that the thalamus is a common site of deactivation during induction by various anesthetic agents (2, 3), that there appears to be a disruption of thalamo-cortical and cortico-cortical connectivity (4, 5), and that specific regions of association cortices show enhanced deactivation with certain anesthetics (6, 7). In parallel with these dynamic interactions, there also appear to be physiologic elements that are invariant and do not change with the loss of consciousness from anesthesia (8, 9). Thus far, these imaging findings, in part due to the limitations of temporal and signal resolution, have yet to be fully integrated with regard to the actual cortical electrophysiology.

EEG provides millisecond resolution of broad cortical changes as measured by electrical potentials acquired from the scalp. Historically, different frequency rhythms have been thought to represent different neural sources. Generally, lower frequency rhythms (<40 Hz) appear to represent thalamocortical circuits (10), whereas the higher frequency rhythms (>40 Hz) arise from intrinsic cortical activity (11). In the setting of anesthesia, EEG-based studies also support that both cortex and thalamus play a role in anesthesia-altered consciousness. John et al. identified that there was an increase in power of low frequencies (<25 Hz) and a decrease in power of high frequencies (25–50 Hz), which was consistent across multiple anesthetic agents and reversible upon recovery (12). This shift in power toward lower frequencies is thought to reflect thalamic hyperpolarization (2). The higher frequencies, or γ-rhythms, are thought to result from small ensembles of cortical neurons firing in synchrony and are associated with higher cognitive operations (13). Thus, their decline with anesthesia has been posited to represent a suppression of cortex, associated with a reduced capacity to integrate information (14). The full scope of the cortical activity revealed with EEG, however, is limited due to the poor spatial resolution, limited frequency bandwidth, and poor signal-to-noise ratio of the signal (15).

To more fully describe the static and dynamic features of the human cortical electrophysiology as patients are pharmacologically transitioned into and out of consciousness, we capitalize on the unique clinical scenario of invasive electrocorticographic (ECoG) monitoring of patients during induction and emergence from propofol anesthesia. By recording electrical activity directly from the surface of the cortex, ECoG provides a powerful method to integrate the spatial, temporal, and spectral features of human cortical physiology not possible with other noninvasive techniques. Although these electrical potentials are acquired from the cortex, the different frequencies appreciable with this technique can be attributed to anatomically diverse neural sources allowing for a broader appreciation of brain dynamics beyond the cortical surface. Given the pharmacologic heterogeneity that mediates the patients' transitions in consciousness (i.e., differences in medications for induction and recovery), we have focused on the physiologic phenomena that are unchanged throughout these transitions, or consistent between transitions, as being indicators of cortical phenomena more relevant to alterations in consciousness rather than to differences in pharmacologic factors. In this study, we show a unique integrated electrophysiologic picture that demonstrates a stable functional architecture that is maintained (irrespective of anesthetic transition), coupled with phased cor-

Author contributions: J.D.B., R.T., and E.C.L. designed research; J.D.B., J.L.R., M.S., C.M.G., Z.V.F., and E.C.L. performed research; J.D.B., R.T., M.S.A., and E.C.L. analyzed data; and J.D.B. and E.C.L. wrote the paper.

The authors declare no conflict of interest.

This article is a PNAS Direct Submission.

[1]To whom correspondence should be addressed. E-mail: LeuthardtE@wudosis.wustl.edu.

This article contains supporting information online at www.pnas.org/lookup/suppl/doi:10.1073/pnas.1011949107/-/DCSupplemental.

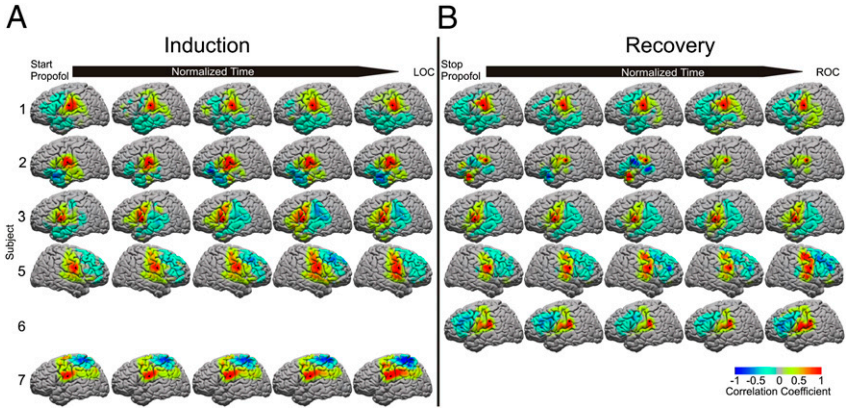

Fig. 1. The SCP somatomotor network is maintained throughout induction and recovery. The correlation of the SCP at all electrodes with a seed electrode on motor cortex is shown in five contiguous nonoverlapping epochs for (*A*) induction and (*B*) recovery. Correlation coefficients are plotted at their respective electrode locations on a standardized Montreal Neurological Institute brain. Distributions generated by epoch subsampling were not statistically different ($P < 0.05$). Subject 4 was excluded because of large seizure foci in the motor cortex; subject 8 was excluded because the grid did not cover the motor cortex.

tical changes that are consistent across heterogeneous pharmacologic transitions in consciousness.

Results

Stability of Slow Cortical Potential (SCP) Networks. The cortical networks defined by correlated SCP (<0.5 Hz) oscillations over the somatomotor cortex remained unchanged throughout induction and recovery. Using an inferior motor cortex electrode seed, confirmed by cortical stimulation mapping, the correlation with all other grid electrodes was computed in five epochs for both induction and recovery (Fig. 1). Subsampling revealed that the correlation patterns from each epoch were statistically unchanged ($P < 0.05$), within subjects, from the initial epoch in all but three instances (subject 3 recovery epoch 2, $P = 0.18$; subject 7 induction epochs 2 and 4, $P = 0.84$ and 0.1). Additionally, these correlation structures were maintained during periods of burst suppression in three subjects from whom burst suppression data were available (Fig. 2).

Absolute Band Power Changes. The absolute band power changes at each electrode are displayed topographically for nine predefined frequency bands in Fig. 3. δ band (1–2 Hz) power demonstrated an increase on induction and a decrease on recovery, whereas the γ1–4 bands (37–205 Hz) were found to have the opposite trends. The γ2–4 bands (75–205 Hz) showed little intersubject or anatomic variability and the changes were statistically significant across subjects as indicated by the 95% confidence intervals ($n = 7$ for induction, $n = 6$ for recovery). The θ (3–8 Hz), μ (9–11 Hz), and β1–2 (13–35 Hz) bands displayed greater intersubject and anatomic variability, with θ and μ showing no significant trends across subjects. β1–2 showed ambiguous behavior during induction, but showed a significant increase in power during recovery. Investigations of relative band power showed similar results (Fig. S1).

Alterations in Power Variance and Covariance. The variance in absolute band power demonstrated temporal behavior that was distinct from that of power (Fig. S2). Whereas the lowest frequencies (δ and θ) showed changes that mirrored their changes in absolute power, the μ through γ1 (9–45 Hz) bands demonstrated significant changes in variance that differed from their absolute power. Fig. 4*A* shows the average μ, β1–2, and γ1 absolute power tracing from an exemplar electrode; there is a notably increased variability in power preceding the loss of consciousness (LOC) (induction) and subsequent to the discontinuation of propofol (recovery). This finding was significant across subjects by bootstrapping the median, as shown in Fig. 5*E* (see Fig. S3 for trends across all bands).

Band power covariance between cortical sites was analyzed for all nine frequency bands, revealing an increase in μ (9–11 Hz), β1–2 (13–35 Hz), and γ1 (37–45 Hz) band-limited power correlation during late induction, before the LOC. During recovery, correlation in these same bands was found to drop just subsequent to the discontinuation of propofol and to remain relatively unchanged to the return of consciousness (ROC) (Fig. 4*B*). The δ and γ4 bands did not reflect these changes in correlation. This trend in μ, β1–2, and γ1 correlation was significant by bootstrapping (Fig. 5*F*) and appears to have similar temporal behavior to the variance trends in this same frequency range (see Fig. S4 for individual subject data).

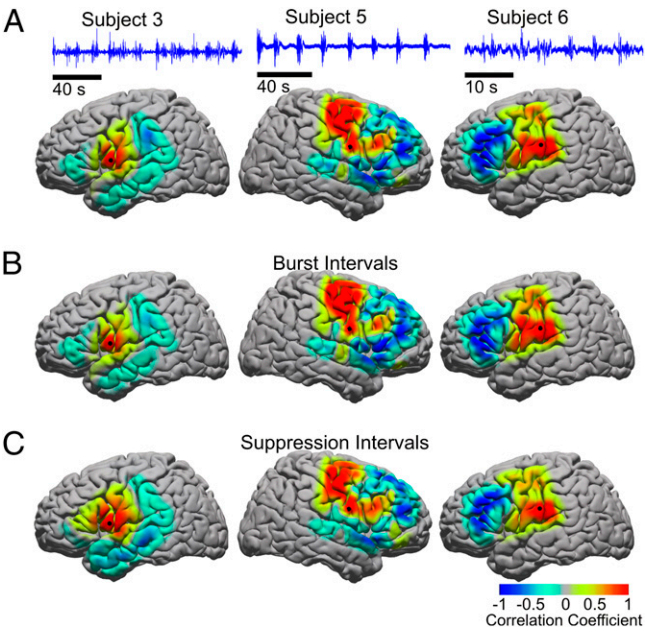

Fig. 2. The SCP somatomotor network is maintained during burst suppression. (*A*) The correlation coefficient of the SCP with a motor cortex seed electrode in three subjects during the period of burst suppression shown (blue trace). Mean correlation structure is shown during (*B*) burst and (*C*) suppression intervals only.

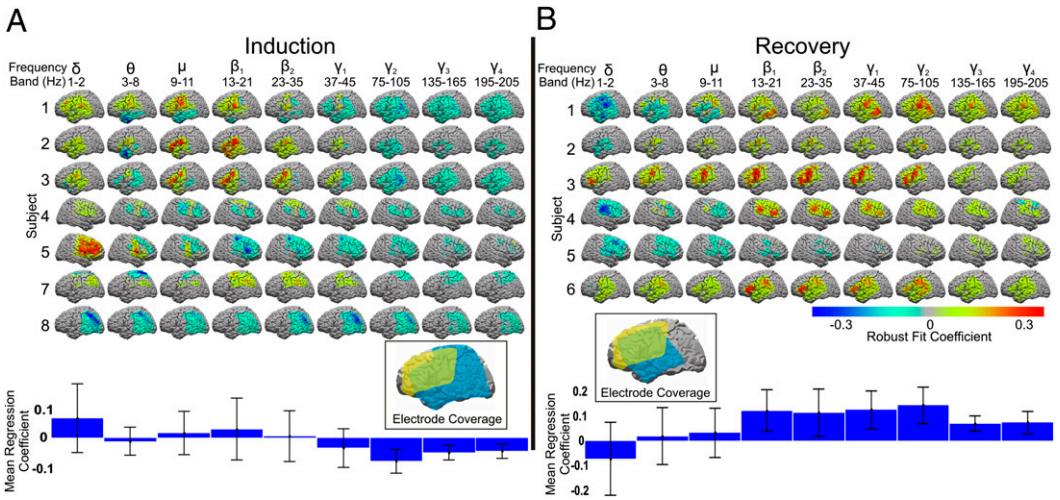

Fig. 3. Topographic absolute power changes during induction and recovery. The robust fit coefficient, or slope ($P < 0.001$), of the absolute band power trend at each electrode during induction (*A*) and recovery (*B*) is shown for the nine frequency bands. The mean and 95% confidence interval across all subjects' electrodes is shown at the bottom. Total electrode coverage is shown in *Insets*. Blue, left hemispheric coverage. Yellow, right hemispheric coverage. Discrepancy in left hemispheric coverage between induction and emergence reflects absence of emergence data from subjects 7 and 8 and absence of induction data from subject 6.

Phase–Power "Coupling" Between Different Frequencies. Relationships between different frequencies were assessed by the correlation between phase and power. A significant ($P < 0.01$) correlation between δ-range (1–4 Hz signal) phase and the β2 through γ3 (23–165 Hz) band power was observed. This correlation appeared to strengthen with induction and diminish during recovery (Fig. 6*A*). Fig. 6*B* illustrates this increased coupling of low-frequency (1–4 Hz) phase to γ-range power with data from a single exemplar electrode. A more finely resolved temporal progression of this phase–power coupling between low and high frequencies can be seen with bootstrapped 95% confidence intervals in Fig. 5*C*. The phase of θ- and μ-range (4–12 Hz) signal oscillations and the power in the γ2–3 (75–165 Hz) bands were found to have a significant ($P < 0.01$) anticorrelated relationship, similar to that described by Canolty et al. (16). This anticorrelation did not appear to change with induction or recovery (Fig. 5*D*) (see Fig. S5 for individual subject data).

Distinct Temporal Dynamics. The temporal relationships of the trends in electrocortical band power, variance, covariance, and phase–power coupling during induction and recovery are summarized in Fig. 5. Piecewise linear regression modeling identified breakpoints within some trends, identifying separable physiologic phases for both induction and recovery from anesthesia (R^2 = 0.135–0.402). Power changes in the δ and γ bands, and coupling between these bands, are the first to occur during induction (Fig. 5, I1), with δ rising and leveling off, whereas γ power shows a continual decrease all of the way to LOC. Following the peaking of δ power and δ–γ coupling, there is increased μ, β1–2, and γ1 variability in power leading up to LOC. This increased waxing and waning of μ, β1–2, and γ1 oscillations is coherent across the cortex, as indicated by the simultaneous rise in μ, β1–2, and γ1 range power covariance between cortical sites (Fig. 5, I2). During recovery, these changes reverse themselves in a similar stepwise fashion. Following discontinuation of propofol, the effects in the μ, β1–2, and γ1 bands reverse themselves; γ power also begins to increase rapidly (Fig. 5, R1). After the μ, β1–2, and γ1 band variance and covariance have reached relatively stable values, the δ power and δ–γ coupling decrease and level off (Fig. 5, R2). Finally, the rate of γ-power increase appears to slow.

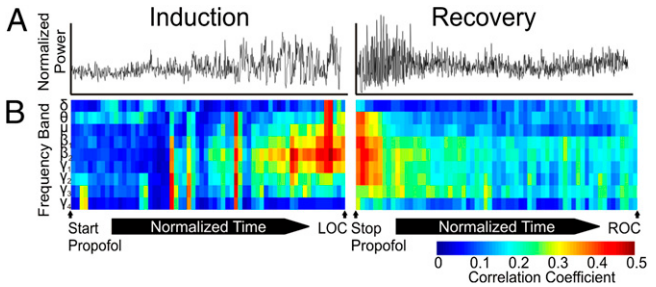

Fig. 4. Trends in μ, β, and γ1 power variability and covariance between distant cortical sites. (*A*) Average normalized μ, β, and γ1 power from an exemplar electrode demonstrating increased variance during induction that decreases on recovery. (*B*) The mean intraband power correlation between electrodes. Power in the μ, β1–2, and γ1 bands shows increasing correlation during induction and a decrease during recovery.

Discussion

This study used invasively acquired electrophysiological signals directly from human cerebral cortex to characterize the changes of both induction and recovery from anesthesia. The distinct frequency-defined cortical phenomena represent either distinct neural sources within the cortex or distant sources having an influence on the cortex. With the loss and recovery of consciousness we report several dominant patterns of the cortical electrophysiology: two that were unchanged with anesthesia and two that were dynamic. The two invariant patterns through anesthesia were the SCP networks and the coupling between θ-phase and high-γ power. The two dynamic patterns were defined by (*i*) δ and high-γ power modulations and (*ii*) μ, β, and low-γ frequency range alterations in power variance and covariance. These dynamic patterns demonstrated a temporal sequence through anesthetic induction that reversed during emergence. These findings support that there are sequential cortical changes that occur with anesthesia-induced changes in consciousness superimposed upon a maintained functional architecture.

Networks defined by correlated and anticorrelated fluctuations of the slowest components of the cortex's electrical potential were found to be stable regardless of the level of anesthesia. Even at very deep levels of anesthesia referred to as burst suppression, where it is commonly thought that consciousness is highly sup-

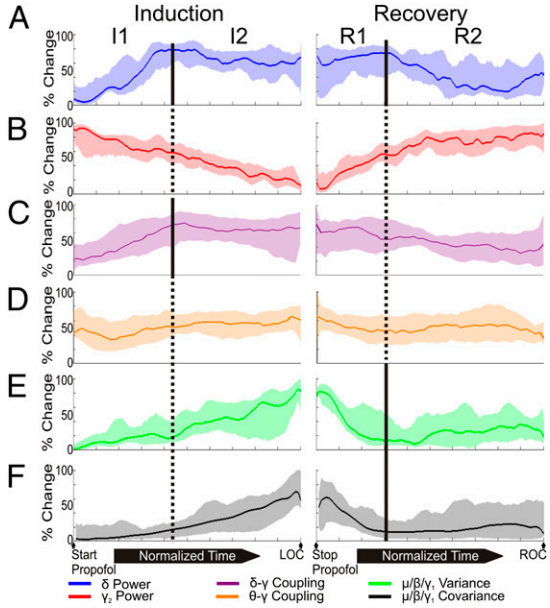

Fig. 5. (*A–F*) Phases of change in spectral power, variance, covariance, and phase–power coupling during induction and recovery. Solid vertical lines demarcate mean knot sites, where segments were found to be separable with adaptive piecewise regression. These demarcations were used to separate the different phases of inductions and recovery. All trends reflect the smoothed median and bootstrapped 95% confidence interval. I1, induction phase 1; I2, induction phase 2; R1, recovery phase 1; R2, recovery phase 2.

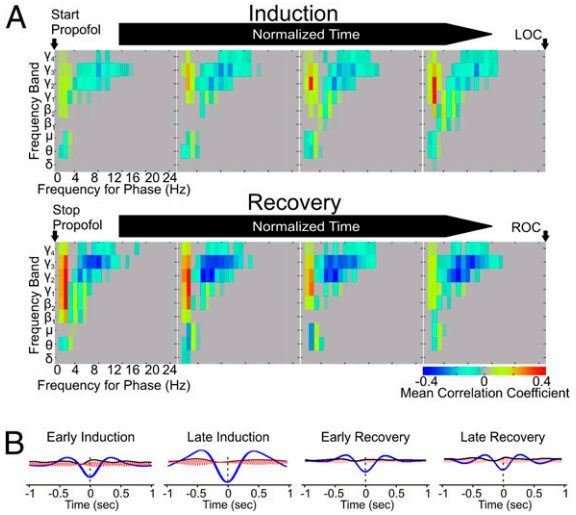

Fig. 6. Phase–power correlations during induction and recovery. (*A*) The mean correlation coefficient across all subjects ($P < 0.01$, Bonferroni corrected) between the signal phase (<25 Hz) and the power in the nine frequency bands. (*B*) Data from an exemplar electrode illustrating the relationship between 1- to 4-Hz phase and high-frequency power that emerges during induction and dissipates on emergence. The average γ2 power fluctuations (black) are increasingly and decreasingly correlated to the phase of the 1- to 4-Hz signal component (blue) on induction and recovery, respectively. High-frequency oscillations (red) illustrate this amplitude modulation.

pressed, the electrically defined somatomotor network was found to be present. These findings are consistent with previous imaging studies of large-scale coherent structures in anesthesia (8, 9). In regard to frequency–frequency interactions, θ–γ coupling first described by Canolty et al. also appeared to be maintained (16). θ rhythms have been closely linked to memory and hippocampal processing (17, 18), and neural information flow from cortex to hippocampus has been demonstrated during sleep (19). This maintained θ–γ relationship may represent preserved organization of hippocampal–cortical interactions persisting through the loss of consciousness and may potentially explain why memories formed before anesthesia are not lost. Taken together, these findings support that there is both an anatomic and a physiologic functional architecture that is maintained throughout induction and emergence, which may be important for the continuity and organization of consciousness that we observe to persist despite transient interruption by anesthetics.

Superimposed on this maintained functional architecture were dynamic electrophysiologic changes that were consistent through the pharmacologically heterogeneous transitions of induction and recovery, respectively. There appears to be an ordered interplay between cortex, thalamus, and the reticular system in progressing in and out of consciousness. With anesthesia there is a steady linear suppression of cortex as manifested by the decline in power in all γ rhythms. The low-γ (30–60 Hz) oscillations are thought to be caused by alternating excitatory and inhibitory postsynaptic potentials (20), whereas the higher oscillatory frequencies >200 Hz are strongly correlated with the summation of action potential spiking (21). Given that propofol acts on $GABA_A$ receptors (22), this global γ decrease supports that cortical neuronal activity is being suppressed by postsynaptic inhibition (23). During this decline, there is an early hyperpolarization of thalamus, evidenced by the early increase in δ power that has been shown to be associated with thalamocortical neurons transitioning from a tonic to a bursting activity pattern (2). With ongoing cortical suppression the fast oscillating cortical neuronal ensembles become progressively entrained by the emerging slow oscillations of thalamocortical circuits, as reflected by the emergence of coupling between γ power and the phase of δ oscillations. These findings are consistent with observations of bistable "up" and "down" states of neuronal activity in anesthetized rat prefrontal and somatosensory cortex (24). In later induction, a spindling-like phenomenon, which is likely originating from reverberating reticulothalamic circuits, seems to arise. These uniform transient oscillations throughout the cortex are reflected by the increase in μ, β1–2, and low-γ variance and covariance across the cortex. Recovery from anesthesia was characterized by a reversal of these cortical changes of induction, namely, a steady increase in cortical activity with an attenuation of reticulothalamic circuits, which was then followed by the return of more tonic activity in the thalamus.

There are limitations of the present study that must be addressed. First, the cortical electrophysiology of epileptic patients may differ from that of the general population due to the presence of seizure foci and the chronic use of anti-epileptics. By normalizing and combining the data across multiple subjects, we likely have accounted for many of these patient-specific elements. A second limitation is the restricted electrode coverage in each patient, which is determined entirely by clinical criteria. Thus, our findings should be interpreted only in the context of the cortical areas covered. Third, we base our SCP network findings on the somatomotor network because of its frequent electrode coverage in the clinical setting. Further invasive electrophysiological studies of other functional networks will reveal if our findings generalize to other networks. Finally, despite the fact that we have identified consistent trends across pharmacologically heterogeneous transitions between conscious states, these trends will need to be identified under other anesthetics to determine whether these changes are more universal.

In conclusion, we report a unique comprehensive recording of invasive human cortical physiology during induction and recovery from propofol anesthesia. Induction is characterized by a two-phased physiologic progression that occurs at distinct frequency scales, whereas emergence from anesthesia involved a reversal of

these two phases. These cortical dynamics associated with the loss and return of consciousness occur in the context of a maintained functional architecture reflected by the correlated fluctuations of the slow cortical potential and maintained θ–γ coupling. This intrinsic functional structure appears to persist in the face of complete suppression of consciousness. These findings provide important electrophysiological evidence in humans of different neuronal mechanisms for maintaining organization in the brain through widespread pharmacologic suppression.

Materials and Methods

Subjects. Eight patients undergoing surgical treatment for intractable epilepsy participated in this study, which was approved by the Human Research and Protection Organization at Washington University School of Medicine. Before inclusion, all patients gave written informed consent. Exclusion criteria included the presence of dysplastic cortex on clinical magnetic resonance imaging. Each patient underwent craniotomy for the subdural placement of an electrode array that was then removed (with a second craniotomy) 1 wk later for resection of the epileptic foci. See Table 1 for demographic and clinical information. See Fig. S6 for intraoperative photo, imaging, and detailed total electrode coverage.

Equipment. ECoG signals were recorded and digitized from the implanted electrode array at a sampling rate of 1,200 Hz, using g.tech biosignal amplifiers. The data were stored by a Dell PC running BCI2000 software (25). The ECoG electrode array (AdTech) contained 48 or 64 platinum electrodes that had 2.3-mm diameter exposed surface and were spaced 10 mm apart.

Data Collection. After closure of the surgical wound, the implanted electrode array was connected to the amplifiers and additional cortical or skull electrodes provided the reference and ground. Skull electrodes consisted of an intracranial electrode strip (1 × 4) that faced the inner table of the skull. A cortical reference was used to avoid the high impedance of a standard skull reference electrode making poor contact due to an immediate postsurgically diminished brain volume. Signal acquisition began when the propofol infusion, used for anesthetic maintenance during the craniotomy, was stopped. Recording continued until the ROC was established (defined as the point when the patient was able to follow a verbal command). One week later, before surgery to remove the electrodes and resect the epileptic foci, data were collected during the induction of propofol anesthesia. The electrode array was connected to the amplifiers, and cortical or skull electrodes provided the ground and reference. Data acquisition began with the start of propofol infusion (Medfusion 2010) and continued until the completion of tracheal intubation. The LOC was noted as the point before intubation when the patient no longer followed verbal commands as described above. Propofol was infused in a continuous and controlled fashion, incrementally titrating up the dose by 50–100 mcg·kg^{-1}·min^{-1} every 3–5 min on the basis of clinical examination. Due to propofol's highly variable effects among individuals (26), this titration was based on clinical observation of spontaneous eye opening, movements, and reaction to environmental stimuli. The bispectral index (BIS) score was manually recorded approximately every 30 s during both the induction and the recovery data collections (Fig. S7). (See *SI Methods* for detailed description of anesthesia protocol and data collection.)

Artifact Removal from ECoG Data. Signals from every electrode were visually inspected and those electrodes identified as having predominately poor signal-to-noise characteristics (amplitude >10^1 times that of the majority of electrodes in the grid) were excluded from further analysis [63 of 320 electrodes (19.6%) from recovery and 20 of 400 electrodes (5%) from induction]. Shorter segments of artifact were manually removed from the remaining signals on the basis of the same criteria (9.9% from recovery and 14.1% from induction). Remaining signals were rereferenced to the common mean. Only recovery signals acquired between the discontinuation of popofol and the ROC, and induction signals acquired between the start of propofol infusion and the LOC, were included in further analysis, with one exception. Burst suppression data collected after the LOC in three subjects were used in analysis of SCP somatomotor network correlation.

Slow Cortical Potential Correlation. To investigate the behavior of the somatomotor network, correlation of the slow cortical potential (>0.5 Hz), shown to be related to fMRI BOLD signal (8), was computed in six subjects with motor coverage. The correlation matrix was computed for five contiguous, nonoverlapping time epochs for induction and/or recovery, and an electrode over the inferior motor cortex was selected as the seed for the somatomotor network. The seed electrode was confirmed to be over the motor cortex by cortical stimulation mapping results. Somatomotor correlation networks were similarly computed for periods of ECoG signal recorded during burst suppression, confirmed on EEG by the anesthesiologist, in three subjects. The average correlation pattern during suppression intervals alone and burst intervals alone was also computed.

To statistically evaluate changes in these somatomotor network correlation structures within subjects over the five epochs of induction and emergence, each epoch was subsampled separately by computing the correlation matrix on contiguous, nonoverlapping 5-s segments within the epoch. For each of these segments, electrodes were classified as being "in network" (correlation coefficient >0) or "out of network" (correlation coefficient <0). A χ^2 test ($\alpha = 0.05$) was used to assess for significant similarity between the somatomotor network correlation patterns of the second through fifth epochs and the initial epoch.

Spectral Power Analysis. Spectral analysis was done by signal convolution with a Gabor wavelet library (27). The time-varying power was computed for frequencies ranging from 0.5 to 205 Hz. A frequency resolution of 1-Hz bins was used <10 Hz, whereas 2-Hz bins were used from 11 to 45 Hz. Above 75 Hz, bins of 5 and 10 Hz were used. Known noise bands at 60, 120, and 180 Hz were intentionally avoided by skipping a 30-Hz-wide band centered on each peak. Analysis was cut off at 205 Hz to avoid an observed 215-Hz noise peak. The spectral power was grouped into nine frequency bands: δ (1–2 Hz), θ (3–8 Hz), μ (9–11 Hz), β1 (13–21 Hz), β2 (23–35 Hz), γ1 (37–45 Hz), γ2 (75–105 Hz), γ3 (135–165 Hz), and γ4 (195–205 Hz). Analysis of trends in the time-varying absolute band power, the relative band power, and the variance in absolute band power followed.

Absolute and relative band power changes over time at each electrode were determined using the MATLAB robust fit algorithm to fit the slope in band power. To cortically localize these power changes at each electrode, the getLOC package for MATLAB was used to estimate the Tailarach coordinates of the electrodes from the lateral skull radiographs (28). Global time-varying trends of the absolute band power were found by smoothing the spectral data from each electrode with a 1-s moving average and down-sampling to one sample/s. For each subject, trends were combined across electrodes by taking the median. These absolute band power trends were then normal-

Table 1. Demographic and clinical information

Subject	Sex	Age	Seizure type	Seizure foci	Duration of Illness, y	Anti-epileptic medications	Induction time, min	Recovery time, min
1	F	44	CP	ATL	36	LTG, TP,	15	21
2	F	49	CP	ATL	48	LTG, TP, ZNA	12	43
3	M	36	CP	ATL	35	DK, TP	14	36
4	M	52	CP	PFL	44	CBZ, DK	16	24
5	F	28	CP	PFL	14	CBZ, CLP, LTG, LA	14	16
6	F	48	CP	ATL	47	DPH, PG	——	14
7	M	27	CP	MPL	26	CBZ, CLP, LTG, PG, DZ	23	——
8	M	21	CP	MPL	9	CBZ, LTG, KP, LA	18	——

ATL, anterior temporal lobe; CBZ, carbamazepine; CLP, clonazepam; CP, complex partial; DK, depakote; DPH, phenytoin; DZ, diazepam; KP, levetiracetam; LA, lorazepam; LTG, lamotrigine; MPL, mesial parietal lobe; PFL, posterior frontal lobe; PG, pregabalin; TP, topiramate; ZNA, zonisamide.

ized by the maximum. Temporal normalization between the standardized endpoints of propofol initiation/discontinuation and LOC/ROC was done after all spectral analysis by dividing by the time to LOC or ROC for induction and recovery, respectively (Fig. S8). The data were then linearly interpolated to equate the number of data points between subjects, which thus allowed for combining data across subjects and bootstrapping the 95% confidence interval.

Power Variance and Covariance. The variance in absolute power was computed for each frequency band and each electrode, using a 30-s sliding window, before temporal normalization. Similarly, intraband covariance trends were analyzed by computing the correlation of the band limited power between all combinations of electrode pairs, using a 30-s sliding window. The median of this time-varying correlation was found across all electrode pairs. Temporal normalization as described above for band power was then performed on the variance and covariance data. Finally, band power variance and covariance data were combined across subjects by finding the median value and bootstrapping a 95% confidence interval at each sample point.

Phase–Power Analysis. The relationship between the phase of lower frequencies ranging from 0.1 to 25 Hz and the power in the nine predefined frequency bands was examined. The raw ECoG signal was bandpass filtered with zero-phase shift for 26 frequency bands (<0.1 Hz, 0.1–1 Hz, and 1–25 Hz in 1-Hz bands), and the filtered signal was subsequently divided into four contiguous nonoverlapping epochs. Within each epoch, segments of the band power and filtered signal were aligned to the troughs of the filtered signal (i.e., aligned to a consistent phase value) with 500-ms lead and lag times. These aligned 1,000-ms segments of band power and filtered signal were averaged separately. The correlation was then computed between the average phase-aligned filtered signal and the average phase-aligned band power. This phase–power correlation was computed for all combinations of the 26 frequency bands for phase bands with the nine frequency power bands, for a total of 234 phase–power relationships. These resulting correlation coefficients were assessed for statistical significance against a distribution of surrogate correlation coefficients, using a standard R^2 comparison. The surrogate data were generated in the same fashion except that they were aligned randomly rather than to a consistent phase value, such that differences between the surrogate data and the phase-aligned data would be explained by real phase–power correlations in the data. A Bonferonni correction for multiple comparisons was imposed. The resulting statistically significant ($P < 0.01$) correlation coefficients were averaged across electrodes for individual patients and then combined across patients by averaging. To resolve the temporal progression of the significant phase–power relationships identified, the correlation between the phase-aligned filtered signal and band power was computed (as described above) using 50 consecutive time epochs. The results were combined across patients by taking the median and bootstrapping a 95% confidence interval.

Piecewise Linear Regression of Trends. The trends in power, variance, covariance, and phase–power coupling were modeled using adaptive piecewise linear regression to identify knots that improved the coefficient of determination (R^2) over a simple linear model. Segments of the model were constrained to be linear and a generalized cross-validation penalty per knot of 10 was used.

ACKNOWLEDGMENTS. We acknowledge the generous support from the Doris Duke Foundation and the James S. McDonnell Foundation.

1. Franks NP (2008) General anaesthesia: From molecular targets to neuronal pathways of sleep and arousal. *Nat Rev Neurosci* 9:370–386.
2. Alkire MT, Haier RJ, Fallon JH (2000) Toward a unified theory of narcosis: Brain imaging evidence for a thalamocortical switch as the neurophysiologic basis of anesthetic-induced unconsciousness. *Conscious Cogn* 9:370–386.
3. Fiset P, et al. (1999) Brain mechanisms of propofol-induced loss of consciousness in humans: A positron emission tomographic study. *J Neurosci* 19:5506–5513.
4. White NS, Alkire MT (2003) Impaired thalamocortical connectivity in humans during general-anesthetic-induced unconsciousness. *Neuroimage* 19:402–411.
5. Ferrarelli F, et al. (2010) Breakdown in cortical effective connectivity during midazolam-induced loss of consciousness. *Proc Natl Acad Sci USA* 107:2681–2686.
6. Kaisti KK, et al. (2003) Effects of sevoflurane, propofol, and adjunct nitrous oxide on regional cerebral blood flow, oxygen consumption, and blood volume in humans. *Anesthesiology* 99:603–613.
7. Ramani R, Qiu M, Constable RT (2007) Sevoflurane 0.25 MAC preferentially affects higher order association areas: A functional magnetic resonance imaging study in volunteers. *Anesth Analg* 105:648–655.
8. He BJ, Snyder AZ, Zempel JM, Smyth MD, Raichle ME (2008) Electrophysiological correlates of the brain's intrinsic large-scale functional architecture. *Proc Natl Acad Sci USA* 105:16039–16044.
9. Vincent JL, et al. (2007) Intrinsic functional architecture in the anaesthetized monkey brain. *Nature* 447:83–86.
10. McCormick DA, Bal T (1997) Sleep and arousal: Thalamocortical mechanisms. *Annu Rev Neurosci* 20:185–215.
11. Gray CM, McCormick DA (1996) Chattering cells: Superficial pyramidal neurons contributing to the generation of synchronous oscillations in the visual cortex. *Science* 274:109–113.
12. John ER, et al. (2001) Invariant reversible QEEG effects of anesthetics. *Conscious Cogn* 10:165–183.
13. Crone NE, et al. (2001) Electrocorticographic gamma activity during word production in spoken and sign language. *Neurology* 57:2045–2053.
14. Alkire MT, Hudetz AG, Tononi G (2008) Consciousness and anesthesia. *Science* 322: 876–880.
15. Nunez P, Srinivasan R (2006) *Electric Fields of the Brain: The Neurophysics of EEG* (Oxford University Press, New York).
16. Canolty RT, et al. (2006) High gamma power is phase-locked to theta oscillations in human neocortex. *Science* 313:1626–1628.
17. Buzsáki G (2002) Theta oscillations in the hippocampus. *Neuron* 33:325–340.
18. Axmacher N, et al. (2010) Cross-frequency coupling supports multi-item working memory in the human hippocampus. *Proc Natl Acad Sci USA* 107:3228–3233.
19. Tononi G, Massimini M, Riedner BA (2006) Sleepy dialogues between cortex and hippocampus: Who talks to whom? *Neuron* 52:748–749.
20. Sukov W, Barth DS (1998) Three-dimensional analysis of spontaneous and thalamically evoked gamma oscillations in auditory cortex. *J Neurophysiol* 79:2875–2884.
21. Jones MS, MacDonald KD, Choi B, Dudek FE, Barth DS (2000) Intracellular correlates of fast (>200 Hz) electrical oscillations in rat somatosensory cortex. *J Neurophysiol* 84: 1505–1518.
22. Krasowski MD, et al. (1998) Propofol and other intravenous anesthetics have sites of action on the gamma-aminobutyric acid type A receptor distinct from that for isoflurane. *Mol Pharmacol* 53:530–538.
23. Edwards E, Soltani M, Deouell LY, Berger MS, Knight RT (2005) High gamma activity in response to deviant auditory stimuli recorded directly from human cortex. *J Neurophysiol* 94:4269–4280.
24. Isomura Y, et al. (2006) Integration and segregation of activity in entorhinal-hippocampal subregions by neocortical slow oscillations. *Neuron* 52:871–882.
25. Schalk G, McFarland DJ, Hinterberger T, Birbaumer N, Wolpaw JR (2004) BCI2000: A general-purpose brain-computer interface (BCI) system. *IEEE Trans Biomed Eng* 51: 1034–1043.
26. Cheng MA, et al. (1996) Large-dose propofol alone in adult epileptic patients: Electrocorticographic results. *Anesth Analg* 83:169–174.
27. Le Van Quyen M, et al. (2001) Comparison of Hilbert transform and wavelet methods for the analysis of neuronal synchrony. *J Neurosci Methods* 111:83–98.
28. Miller KJ, et al. (2007) Cortical electrode localization from X-rays and simple mapping for electrocorticographic research: The "Location on Cortex" (LOC) package for MATLAB. *J Neurosci Methods* 162:303–308.